

Zhiguang Cheng
R & D Center, Tianwei Group Co., LTD, CHINA,
emlab@btw.cn

Behzad Forghani
Infolytica Corporation, CANADA,
forghani@infolytica.com

Norio Takahashi
Dept. of E.E., Okayama University, JAPAN
norio@elec.okayama-u.ac.jp

Xiaoyan Wang
R & D Center, Tianwei Group Co., LTD, CHINA,
wangxiaoyan@btw.cn

ENGINEERING-ORIENTED BENCHMARKING AND APPLICATION-BASED MAGNETIC MATERIAL MODELING IN TRANSFORMER RESEARCH

SUMMARY

The paper highlights the engineering-oriented benchmarking and application-based magnetic material modeling, as two important events in transformer research, reviews the newly extended progress in TEAM (Testing Electromagnetic Analysis Methods) Problem 21 Family, and presents the related benchmarking results.

Key words: Application-based magnetic material modeling, engineering-oriented benchmarking, finite element, industrial application, Iron loss, magnetic flux.

1. INTRODUCTION

The effectiveness of the numerical modeling is essentially dependent on the analysis method, software being used, and the sufficient material property data. Consequently, the validation of both the numerical computation and the material property modeling becomes two important events.

In order to validate the numerical modeling, since 1985, the international COMPUMAG (biennial conference on the computation of the electromagnetic fields) society has paid great attention to organize the TEAM activities worldwide to test and compare the electromagnetic analysis methods, and established a series of benchmark problems widely used in the computational electromagnetics community [1]. Meanwhile, the IEEE Standard for validation of computational electromagnetics computer modeling and simulations has been issued [2]. The authors have made efforts to the engineering-oriented TEAM activities for years [3-13], also proposed a benchmark family, Problem 21[1], and updated it for three times since 1993, many scientists and engineers are interested in it up to now.

On the other hand, the more advanced material modeling techniques have been investigating systematically [14]. As a result, there has been significant progress in the efficient design of electromagnetic devices [15-18]. However, so far, what being widely used in industrial application is the standard one-dimensional B-H curves, obtained from either the Epstein frame or the single sheet tester (SST), and B-H properties change according to the working conditions, e.g. they could vary with the frequency, the temperature, and the stress action. Therefore, it is necessary to validate the availability of the B-H property data when modeling a device under working conditions.

In very large electromagnetic devices, for example a large power transformer, the reduction of stray-field loss, produced by the leakage flux from the transformer winding and heavy current leads, and

the protection against unallowable loss concentrations and then local over heating have become more and more significant[19-25]. Various types of power frequency shields are widely utilized to effectively save energy and ensure a reliable operation. In addition, the various shields can change and control the global distribution of the 3-D electromagnetic field within a large device. It is important to accurately model the multi-shielding effects and optimize shielding configurations at the electromagnetic design stage, but not use rough estimates [20-21].

The purpose of this paper is to focus on the engineering-oriented benchmarking and the application-based magnetic material modeling in power transformers, examine the effect of the variation in the different B-H representations used in different solvers on iron loss and flux in GO(grain-oriented) silicon steel sheets, and investigate the power frequency multi-shielding effect based on shield models. In addition, an improved method for measuring stray-field loss is proposed, and validated based on a newly designed benchmarking set up, making use of two leakage flux complementary coils.

2. ENGINEERING-ORIENTED BENCHMARKING

The electromagnetic and thermal field problems in large power transformers are usually very complicated, which involve multi-physic field coupling, multi-scale (very thin layer and very large bulk) components, and multi-materials varying with the working conditions. In order to obtain an effective solution, the strict validation of the analysis method and software used for solving such complex field problems are certainly necessary. However, it is impossible to do that via a large real product. Therefore, the verification based on the engineering-oriented benchmark models becomes a best way.

To investigate the stray-field loss problems in power transformers, a benchmark family, TEAM Problem 21 of 16 benchmark models, has been well established (the definition of Problem 21, v.2009, can be found at www.compumag.org/TEAM)[1], and a number of benchmarking results have been presented by the authors and the researchers worldwide[4]. All the benchmark models come from the typical structures of power transformers, presenting different electromagnetic behavior, and the engineering-oriented benchmarking activities have the following characteristics:

a) **Test electromagnetic analysis methods**

The original motivation of benchmarking (TEAM) is to test the analysis method and computation software, including the commercial software being in use, and is a regular topic of the international COMPUMAG conference.

b) **Verify computation models**

It is important to build up a correct numerical computation model, such as, taking the nonlinearity, electric and magnetic anisotropy of material, skin effect and loss concentration in components into account, and involving the reasonable simplification treatment for reducing the computation cost.

c) **Detail the field behavior of typical product structure**

Problem 21 is transformer-oriented, including transformer tank, core-plate, and shielding models. The detailed modeling of the stray field loss generated in different components and the electromagnetic field distributions will be helpful to improve product design.

d) **Benefit to large-scale numerical modeling**

Benchmark model is different from a large product, but the benchmarking results will be useful to solve large-scale field problems in the simplification of practical problem, the treatment of material properties, and the choice of the solvers.

Table 1 shows the benchmarking notes concerning with TEAM Problem 21, which is expected to be helpful for the numerical modeling in power transformers.

3. APPLICATION-BASED MAGNETIC MATERIAL PROPERTY MODELING

From the point of view of industrial application, both keeping track of advanced material modeling technologies and promoting the large-scale application using the existing material property data are really important and challenging.

Table 1 Benchmarking notes

P21 ^o	In the iron-loss calculation, the hysteresis loss component and the nonlinearity of the magnetic steel must be accounted (P21 ^o includes Model A and Model B of Problem 21).
P21 ^a	The satisfied results of eddy current losses in non-magnetic steel can be achieved using different 3-D analysis methods based on different potential sets, even with coarse mesh in non-magnetic components, but 2-D results is not available.
P21 ^b	The detailed examination and comparison of both the total loss and the loss concentration in the hybrid steel plate structure are of importance to improve the product design.
P21 ^c	The evaluations of the power loss and magnetic flux inside both electromagnetic and magnetic shields, as well as that of the separation-type shields, are given.
P21 ^d	Both the iron loss and magnetic field inside the GO silicon steel lamination with different excitation patterns, and the additional iron loss induced by normal magnetic flux are detailed.

a) **A bottleneck problem of industrial application**

The material property modeling is one of the key topics of this Colloquium, also is another regular topic of COMPUMAG. In author's opinion, it still is a bottleneck-problem of industrial application. This is because that, the measurement conditions of the material properties were standard, using the standard equipments, such as, Epstein frame, SST, or other equipments to be applied for getting vector magnetic properties, however, the working conditions of the components and device are not standard.

Up to now, the material property data provided by the material providers are one-dimensional, but the field problems in the real products are three-dimensional. So another problem is that how to use the existing property data to solve the practical problems?

b) **Combination of material modeling and numerical computation**

Most of the current electromagnetic-thermal analysis software can access the one-dimensional or the so-called orthogonal-anisotropic property data. A natural problem is that the software must be upgraded if the vector property data of the material is to be used.

c) **Improvement of magnetic property modeling technology**

Since many years ago, the standard testing equipments used for the magnetic material property modeling are commonly used. The extension of the measurement function and the updates of the setting value with the tester are necessary. For example, using Epstein frame to measure the different type of B-H curves (B_m - H_m and B_m - H_b), the mean path length of the Epstein is varied with many factors but not a constant values [14,26].

4. MAGNETIC PROPERTY MODELING OF GO SILICON STEEL SHEETS

4.1. Different B-H curves

Two kinds of B-H curves, namely B_m - H_m and B_m - H_b , are currently used in electromagnetic field computation[11]. The B_m - H_m curve takes the maximum values of both the flux density (B_m) and the magnetic field strength (H_m) within a cycle. Generally, B_m and H_m cannot achieve the maximum value at the same time inside the magnetic steel due to the eddy current, especially at low flux density, as shown in Fig.1. Thus there is another magnetic field strength H_b corresponding to the maximum value of the flux density B_m , i.e. B_m - H_b curve, see Fig.1. The eddy current becomes zero at the instant when the flux becomes the maximum, therefore, B_m - H_b curve can be referred to as a dc B-H curve.

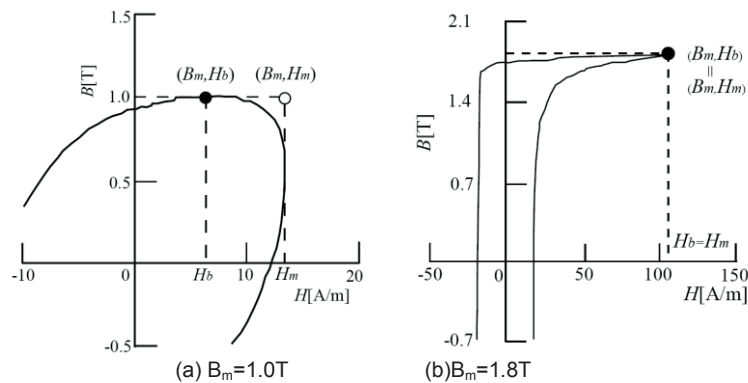


Fig.1. Definition of B_m , H_m and H_b (30P105, $f=50\text{Hz}$).

Fig.2 shows the examples of forming B_m-H_m and B_m-H_b curves based on hysteresis loops (30P105), and Fig.3 demonstrates the measured B-H curve family (SST with H coil) at different frequencies. Both Fig.2 and Fig.3 indicate that the B_m-H_b curves at around a commercial frequency (e.g., 50Hz) are similar to the dc B-H curve at low frequency (0.01Hz), but B_m-H_m curves are different from the quasi dc B-H curve.

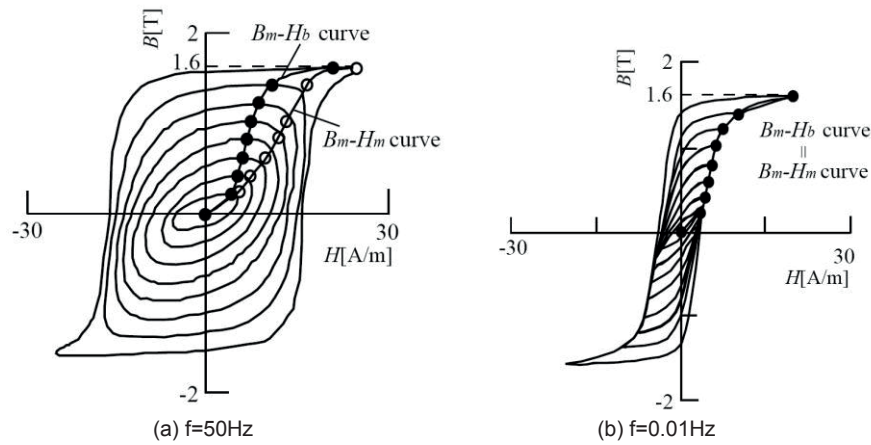


Fig. 2. Hysteresis loops at different frequencies (30P105).

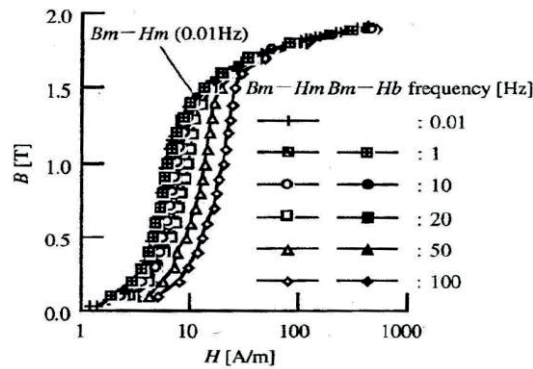


Fig.3. Comparison of B-H curves (30P105).

4.2. Different sampling of GO silicon steel sheets

The magnetic property data of the GO silicon steel sheets 30P120 (made in Korea) are measured using Epstein frame, at the different sampling angles to the rolling direction and the different excitation frequency, as shown in Fig.4 [11].

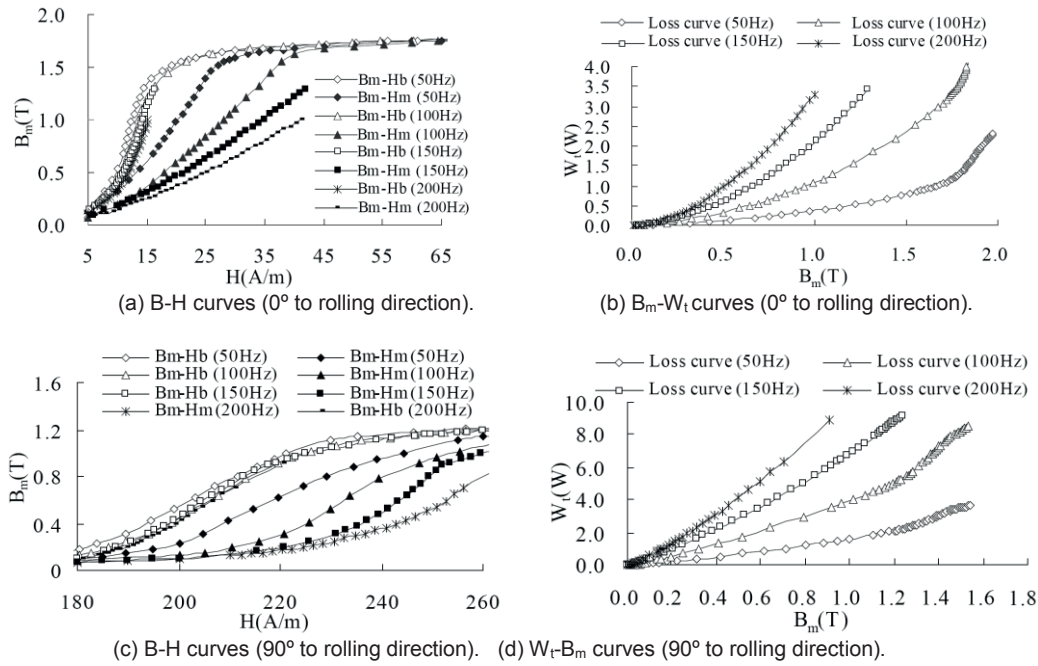


Fig.4. B-H and B_m - W curves of 30P120.

A comparison between the B-H curves, i.e., B_m - H_m and B_m - H_b , measured by using Epstein frame and SST respectively, is given. See Fig.5.

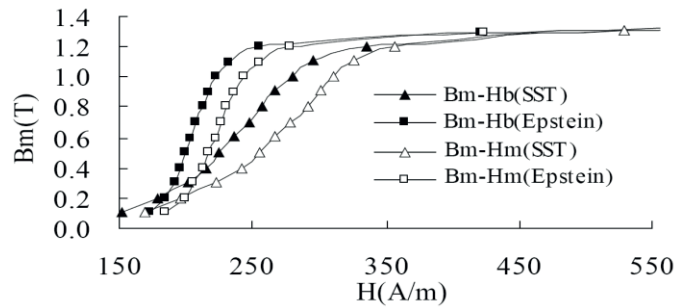


Fig.5. B-H curves (90° to rolling direction) measured using SST and Epstein frame (30P120).

4.3. On the mean path length of Epstein frame

The mean path length of the Epstein frame (25 cm) is constant, 0.94m, in the IEC standard [26], it has found that the mean path length is dependent on many factors, and is not always equal to 0.94m. This paper shows the further experimental study, using two Epstein frames (i.e., standard 25cm and revised 17.5cm Epstein frame) regarding it. The field and loss distributions at the corner areas of the two Epstein frames are kept identical, and only the difference between two frames is in length of the Epstein limb, is a basic assumption.

The mean path length of the Epstein frame can be determined based on the specific total loss produced in the middle portions of the Epstein limb [26], denoted by l_{m1} , i.e., eliminating the effect of the Epstein corners on the specific total loss obtained based on two Epstein frames. However, the specific total losses at the limbs (P_{loss1}) and the corner areas (P_{loss2}) of the whole Epstein limb are different.

In order to define an actual mean path length of the Epstein frame (denoted by l_e), both the contributions from the middle portion of the limbs and the rest of the whole frame, including the 4 corner laps, should be taken into account. For this reason, two things done by the authors are as follows:

- 1) The mean path lengths are defined by two methods, i.e., two kinds of the mean path lengths, l_{m1} and l_{m2} were determined by the specific loss of the middle part of the limbs and that of the rest of the whole frame, respectively.

- 2) A weighted processing method for the above mean path lengths is proposed, i.e., the resulting mean path length l_e is treated as a weighted sum of l_{m1} and l_{m2} , incorporating the weight factors α and β respectively, as shown in (1),

$$l_e = \alpha \cdot l_{m1} + \beta \cdot l_{m2} \quad (1)$$

where

$$\alpha = \frac{P_x}{P_x + P_y}; \beta = \frac{P_y}{P_x + P_y}; P_x = \frac{1}{P_{limb}}; P_y = \frac{1}{P_{corner}}$$

The weighted mean path lengths of Epstein frame (25 cm), according to (1), have been determined under different sampling angle to the rolling direction, as shown in Figs.6-8.

It can be seen that, l_{m1} and l_{m2} are quite different and varying with the flux densities, however the weighted mean path length l_e is in between l_{m1} and l_{m2} , and l_e is close to 0.94m, 0.92m and 0.93m at the sampling angle 0° , 55° , and 90° , respectively.

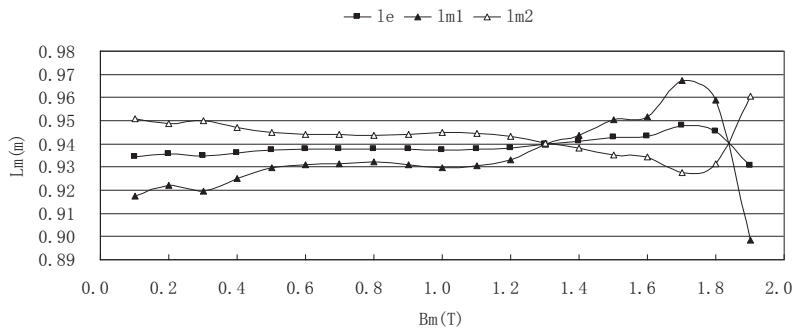


Fig.6 The mean path length determined by different methods(1)
(30P120, 0° to the rolling direction, 50Hz)

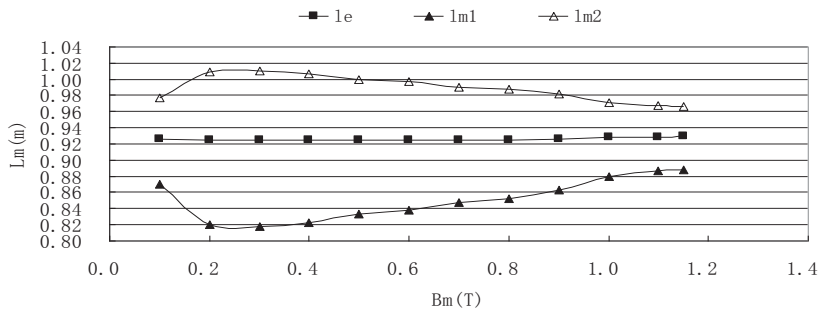


Fig.7 The mean path length determined by different methods(2)
(30P120, 55° to the rolling direction, 50Hz)

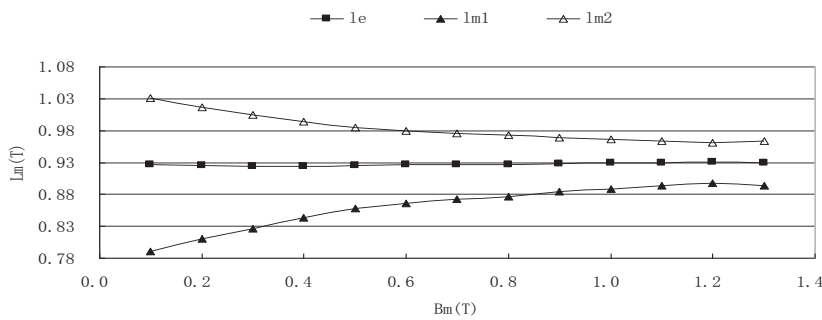


Fig.8 The mean path length determined by different methods(3)
(30P120, 90° to the rolling direction, 50Hz)

Notes for Figs.6-8:

l_e : weighted length based on specific total loss at both limb and corner;

l_{m1} : length based on specific total loss at limb;

l_{m2} : length based on specific total loss at corner area.

5. FE MODEL FOR LAMINATION CONFIGURATION

In order to reduce the computation costs and obtain the efficient solutions, many homogenization treatment methods of the lamination structures, such as, transformer core and magnetic shields, have been proposed [27-32]. The following benchmarking issue aims to deal with the standard iron loss and additional iron loss based on the simple model [10].

5.1. Finite element model

The simplified finite element model of the laminated GO silicon sheets has the following characteristics:

1) Treatment of electric anisotropy

Pattern 1: Modeling the first few laminations individually and modeling the rest as bulk; 3-D eddy currents flow in the individual laminations and 2-D eddy currents limited in each lamination in the bulk region where the anisotropic conductivity is used, see Fig. 9(a).

Pattern 2: Fine meshing within a thin surface layer, and coarse meshing inside the bulk. In the entire conducting domain the anisotropic conductivity is assumed. See Fig.9 (b).

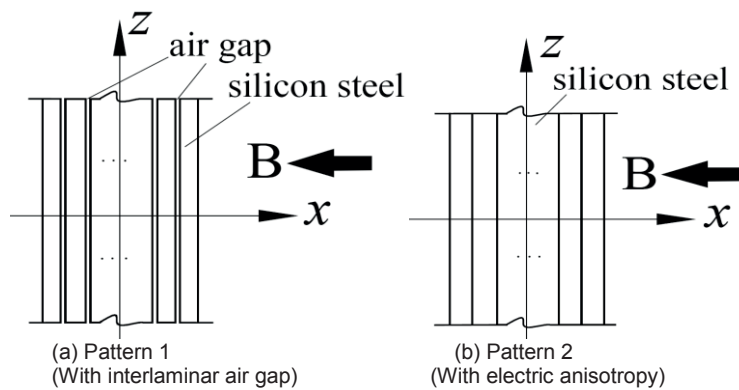


Fig.9. Simplification of laminated sheets.

2) Treatment of magnetic anisotropy

The resulting magnetic field inside the laminated sheet models is almost in one direction (along z-axis), making it a weak magnetic anisotropy problem, and the orthogonal anisotropic permeability is assigned in all the laminations.

5.2. Eddy current analysis

The well-established eddy current solvers based on various potential sets have been developed and applied in the computational electromagnetics and industry [33-37]. The \mathbf{T} - Ω potential set-based method is used in this paper, in which the magnetic field represents as the sum of two parts, i.e., the gradient of a scalar potential Ω and \mathbf{T} , in the conductors, an additional vector field represented with vector-edge elements. As a result, the solution vector consists of the magnetic scalar potential at the nodes plus edge-degrees of freedom associated with the current flow in solid conductors. The \mathbf{T} - Ω based solver does not run into the convergence and instability issues associated with other formulations [36]. The governing equation in the eddy current region, in which involving anisotropic and nonlinear materials, is given by (2),

$$\nabla \times ([\sigma]^{-1} \nabla \times \mathbf{T}) + [\mu] \frac{\partial (\mathbf{T} - \nabla \Omega)}{\partial t} = 0 \quad (2)$$

The anisotropic and nonlinear permeability $[\mu]$ of (2) can be represented by (3)

$$[\mu] = \begin{bmatrix} \mu_0 / (1 - c_p) & & \\ & C_p \mu_y & \\ & & C_p \mu_z \end{bmatrix} \quad (3)$$

where: C_p is the packing factor.

The anisotropic conductivity $[\sigma]$ of the sheets can be dealt with as

$$[\sigma] = \begin{bmatrix} c_p \sigma_x & & \\ & c_p \sigma_y & \\ & & c_p \sigma_z \end{bmatrix} \quad (4)$$

where: $\sigma_y = \sigma_z = \sigma_{yz}$ in sheets, while σ_x is expressed as

$$\sigma_x = \begin{cases} \approx 0 (2D \text{ eddy current region}) \\ \text{assigned} (3D \text{ eddy current region}) \end{cases} \quad (5)$$

The iron loss and flux generated in the GO laminations are computed based on the field analysis results of the eddy current field as part of the post processing. The additional iron loss P_a caused by the flux normally entering the laminated sheets can not be neglected. As a practical solution, the total iron loss P_t can be divided into two parts, i.e.,

$$P_t = P_a + P_s \quad (6)$$

where: P_s can be determined based on the measured loss curve Bm-Wt, and P_a can be calculated based on the field results of 2-D eddy current J_{yz} flowing in the plane of the lamination by (7),

$$P_a = \int \frac{\overline{J_{yz}}_{rms}^2}{\sigma_{yz}} dV \quad (7)$$

Note that the standard specific iron loss P_s includes all the loss components, i.e. the classical eddy current loss $P_e^{classic}$ and the anomalous eddy current loss P_e^{anomal} and the hysteresis loss P_h ,

$$P_s = P_e^{classic} + P_e^{anomal} + P_h \quad (8)$$

The magnetic flux inside GO silicon sheets can be determined by integrating the calculated flux densities over the specified cross-sectional areas or based on the measurements using the search coils.

6. EFFECT OF B-H PROPERTIES ON IRON LOSS AND FLUX

6.1. Test models

To examine the effects of the different B-H representations on the iron loss and flux inside the lamination, two test models have been proposed, i.e. Model T1 and Model T2, which are derived from the benchmark Model P21^c-M1 and P21^c-M2 of Problem 21 Family, respectively. The brief comparisons among the benchmark models and the newly proposed Problem 21-based test models are shown in Table 2.

In Model T1, only six silicon steel sheets of 500×500mm (30P120) are driven by a twin AC source (50 to 200Hz), a 3-D excitation, see Fig.10(a). The purpose of Model T2 is to show the effect of the division of the wide sheets on the reduction of iron loss, see Fig.10(b).

Table 2 Specification of test model and benchmark model

Models	Magnetic plate of 10 mm thick	GO silicon sheets	Sheet-coil distance (mm)	Sheet size (mm)
T1	Without	30P120	15.0	500×500
T2	Without	30P120	12.0	80×458 (3 sets)
P21 ^c -M1	With	30RGH120	12.0	270×458
P21 ^c -M2	With	30RGH120	12.0	80×458 (3 sets)

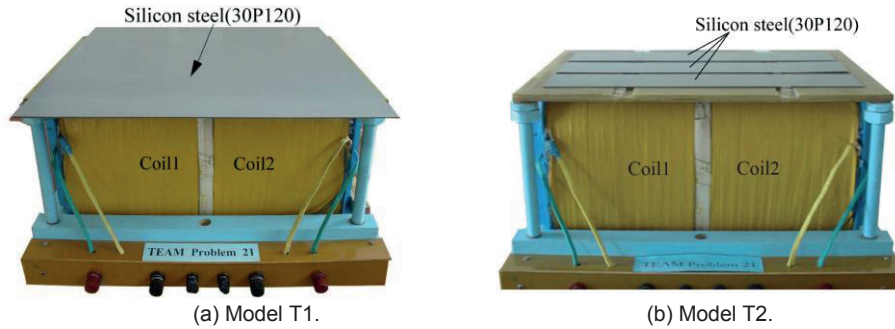


Fig.10. Models T1 and T2.

The B-H curves (B_m - H_m and B_m - H_b) and the specific loss curve (W_t - B_m), measured at different sampling angles to the rolling direction of the GO steel sheet (30P120) and at different frequencies using the Epstein frame, are shown in Fig.4 [11].

6.2. Results and discussion

According to the pre-measurement results obtained by the authors, the saturation level of the laminated sheets is not so high, especially at lower excitations. Both the time harmonic (TH) and the time stepping (TS) solvers of the T - Ω -based MagNet, Infolytica, are used to solve the 3-D eddy current problem. Table 3 shows the calculated and measured results of total iron loss P_t of Model T1.

All the calculated results, using different B-H curves and different solvers, indicate that the use of TH solver and B_m - H_m curve can offer the better results when compared to measurement. This is, because the element-permeability is dependent on the quasi-maximum values of B and H within a cycle in the TH solver. On the contrary, in the case of the TS solver, B_m - H_b curve can offer the better results. This is, because in the TS solver the element-permeability is determined according to the instantaneous values of B and H at an instant. As a result, a more precise analysis is possible by the time stepping method using the B_m - H_b curve, which is almost the same as the dc B-H curve.

Table 3 Total iron loss results (Model T1)

Current (A, rms, 50Hz)	Calc. (W)				Meas. (W)
	TH solver/Pattern 1		TS solver/Pattern 2		
	B_m - H_b	B_m - H_m	B_m - H_b	B_m - H_m	
10	2.61	2.74	2.54	2.35	2.52
15	7.26	7.89	6.66	6.24	7.12
20	12.74	14.14	13.37	12.65	13.7
25	20.31	22.47	23.68	24.01	23.8

Table 4 shows the contributions of additional iron loss P_a and standard specific iron loss P_s to the total iron loss P_t , using different solver and/or different kinds of B-H curves. Table 4 also indicates that P_s calculated using B_m - H_b curve is larger than that using B_m - H_m curve. This is, because the permeability taken from B_m - H_b curve is higher than that taken from B_m - H_m curve. See Fig.4.

However, from the calculated results, P_a has a different tendency, using different B-H curve and/or different (TH or TS) solver.

Table 4 Components of iron loss (Model T1)

Current (A, rms, 50Hz)	TH solver (W)				TS solver (W)			
	B _m -H _b		B _m -H _m		B _m -H _b		B _m -H _m	
	P _a	P _s						
10	1.53	1.08	1.81	0.93	1.73	0.81	1.72	0.63
15	5.50	1.76	6.35	1.54	5.20	1.46	5.12	1.12
20	10.44	2.31	12.07	2.07	11.15	2.22	10.95	1.70
25	17.19	3.12	19.89	2.58	21.22	2.46	21.59	2.42

The calculated results by both the TH and TS solvers show that the iron loss is mainly concentrated in a few layers on the side facing the exciting source, and goes down with the increase of layer-number going from 1 to 6, at 20A(50Hz) for Model T1, as shown in Fig.11.

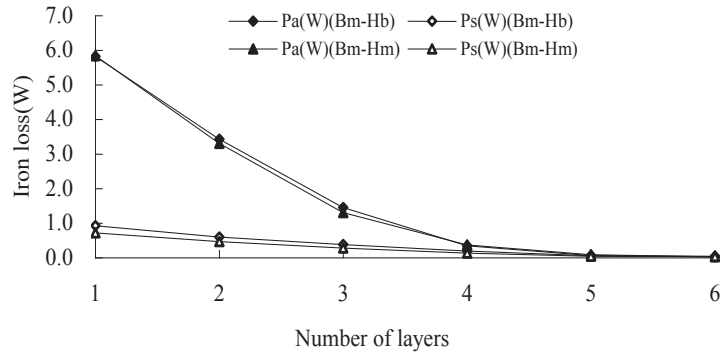


Fig.11. Iron loss distribution in layers (calculated by TS solver, Model T1, at 50Hz).

To determine the magnetic flux inside the laminated sheets, the search coils are set up in Model T1, see Fig.12(a). The magnetic fluxes, at the prescribed positions of the laminations under the different exciting currents, are calculated. Either TH solver and B_m-H_m curve or TS solver and B_m-H_b curve are applied. The calculated results agree well with the measured ones. See Fig.12(b).

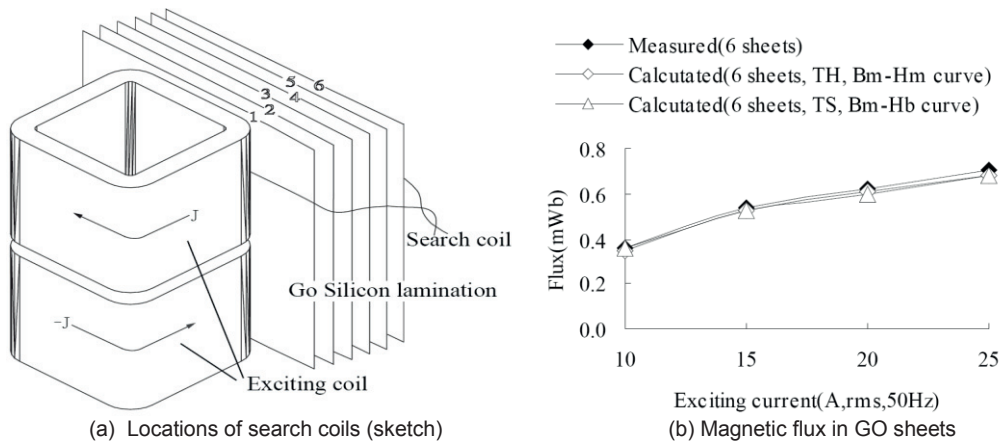


Fig.12. Magnetic flux inside GO laminated sheets (Model T1, 50Hz).

In Model T2, the iron loss produced in the three sets of the narrow GO silicon steel sheets of 80×458mm, which are placed in parallel, is considerably lower compared to that of Model T1 for the same exciting currents.

Fig.13 shows the calculated and the measured results of iron loss of Model T2 at 10A, under a frequency range from 50 to 200Hz. The results also denote that the iron loss increases with the exciting frequency.

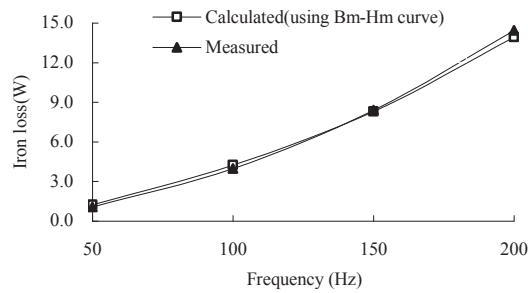


Fig.13. Iron loss varying with frequency (calculated by TH solver using B_m - H_m curve, Model T2).

A very briefly summary is as follows:

- 1) The examination of the effect of the different B-H curves (obtained by different means and data access modes and at different frequencies) on iron loss and flux in GO silicon steel laminations is carried out. The numerical modeling results of the iron loss and flux based on the test models are practically in agreement with measured ones.
- 2) All the numerical modeling results suggest that the B_m - H_b curve is desirable for the use in the transient solver, but the combination of the B_m - H_m curve and the time harmonic solver is also available for the problem with lower saturation level.
- 3) The additional iron loss (P_a) due to the normal flux exponentially drops from the surface facing the exciting source to the opposite side of the laminated sheets. On the other hand, the specific iron loss (P_s) generated by the parallel flux drops slowly compared to P_a .

7. IRON LOSS EXPERIMENT WITH MAGNETIC FLUX COMPENSATION

The electromagnetic (EM) barrier, the magnetic (M) shunt and a combination of both are widely used in electrical devices in order to control stray fields and effectively reduce the power loss that may lead to hazardous local overheating. The hybrid (M+EM) shielding behavior of the current magnetic shunt configuration is numerically and experimentally examined, and compared to other types. The leakage flux complementary-based measurement method of stray-field loss is also proposed and verified based on the benchmark shielding models.

7.1. New generator and compensator of leakage flux

The authors have upgraded the original leakage flux generator (E-coils 1 and 2) specified in TEAM Problem 21 to product-level M- and MEM-type shields. The main change is the increase of the number of turns in the exciting coil (from 300 to 400) and the dimension of the copper wire (from 6.7mm×2mm to 9mm×3mm).

The leakage flux of the exciting coils changes when the magnetic components are removed (as in the no-load case) from the assembly shield models, especially, in the case of the elevated excitation. To keep the leakage magnetic field (reflecting the M- and EM shielding effects) of the exciting coils from changing under the “no-load” condition, two complementary coils (called the C-coils) are utilized, which have completely the same specification as the generator coils (E-coils), and are movable in parallel rails, as shown in Fig.14.

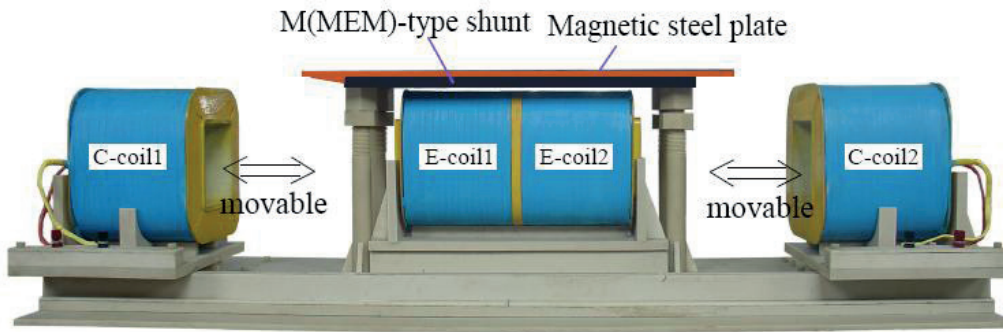


Fig.14. Shield loss measurement with C-coil (photo).

Accordingly, in the no-load (i.e., the magnetic components are removed) case, two C-coils are attached in the main assembly and are located in a symmetric position with respect to the twin exciting coils. However, in the load (i.e., the magnetic components are attached) case, the two C-coils are separated off. See Fig.14.

7.2. Transformer-based shielding models

Fig.15 shows two kinds of magnetic shunt components. The dimensions of the steel plate (A3) are 500×1000×10(mm) and the property data are available in the definition of TEAM Problem 21. In the M- and MEM-type shields, the GO silicon steel, 30P120, is used. The external dimensions of both the M- and MEM-type shunt are 200×860×20(mm).

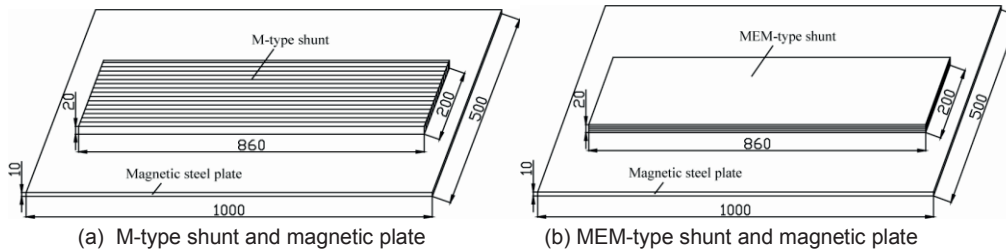


Fig.15. M- and MEM-type shields.

Table 5 shows the calculated and measured results of iron loss, generated in the magnetic component of MEM-type shield. The agreement between the calculated and measured results for total iron loss is satisfied when the C-coils are used. However, the measured results without the C-coils are not acceptable for the proposed shielding models.

Table 5 Iron loss in components of M-type shield

Currents (A,rms)	Calculated iron loss(W)			Measured iron loss(W)	
	Loss in shunt	Loss in plate	Total Loss	With C-coil	Without C-coil
5	0.032	0.370	0.402	0.40	1.24
10	0.13	1.33	1.46	1.45	4.79
15	0.29	3.10	3.39	3.45	10.52

Note that the differences between the iron-loss results of M- and MEM-type shields caused mainly by the loss produced in the magnetic shunt, and the losses in the magnetic plate are almost the same, based on the present results shown in Tables 5 and 6.

Table 6 Iron loss in components of MEM-type shield

Currents (A,rms)	Calculated iron loss(W)			Measured iron loss(W)	
	Loss in shunt	Loss in plate	Total loss	With C-coil	Without C-coil
5	0.37	0.35	0.72	0.70	1.52
10	1.49	1.43	2.92	2.95	6.25
15	3.91	3.05	6.96	7.06	14.81

8. CONCLUSION

The engineering-oriented benchmarking and the application-based magnetic material modeling, which are two important events in transformers research and industrial application, are highlighted in this paper, including some Problem 21-based new benchmarking results and some new material modeling results of magnetic properties.

The effect of the variation in the different B-H representations used in different solvers on iron loss and flux in GO silicon steel sheets are examined in detail, and the power frequency multi-shielding effect based on shield models are investigated. The measurement method of stray-field loss is improved and validated based on a newly designed benchmarking set up.

ACKNOWLEDGMENT

The authors would like to thank the heads of the R & D Center, BTW, Q.Ding, C.Jiang, C.Fan, and X.Zhang, thank the colleagues, L.Liu, Y.Fan, T.Liu,Q.Hu, J.Zhang, J.Wang, J.Li and Q.Kong for their support and help in the long-term experiment and numerical modeling. The project was supported in part by the Natural Science Foundation of China under Grant No.50777042, and the China Postdoctoral Science Foundation under grant No. 2011M500534.

REFERENCES

- [1] TEAM Benchmark Problems. [Online]. available: www.compumag.org/TEAM.
- [2] IEEE Std 1597.1TM-2008: IEEE Standard for validation of computational electromagnetics computer modeling and simulations.
- [3] Z.Cheng,Q.Hu,S.Gao,Z.Liu,C.Ye, M.Wu, J.Wang, and Z.Hu, "An engineering-oriented loss model (Problem 21)," Proc. of the international TEAM Workshop, Miami, pp.137-143,1993.
- [4] Z.Cheng, Q.Hu, N.Takahashi, and B.Forghani, "Stray-field loss modeling in transformers," *International Colloquium Transformer Research and Asset Management*, Cavtat, Croatia, Nov.12-14, 2009.
- [5] N.Takahashi, T. Sakura and Z. Cheng, "Nonlinear analysis of eddy current and hysteresis losses of 3-D stray field loss model (Problem 21)," *IEEE Trans. on Magn.*,vol.37, no.5, pp.3672-3675, 2001.
- [6] Z.Cheng, R. Hao, N. Takahashi, Q. Hu, and C. Fan, "Engineering-oriented benchmarking of Problem 21 family and experimental verification," *IEEE Trans. on Magn.*, vol. 40, no.2, pp.1394-1397, 2004.
- [7] Z.Cheng, N. Takahashi, S. Yang, T. Asano, Q. Hu, S. Gao, X. Ren, H. Yang, L. Liu, and L. Gou, "Loss spectrum and electromagnetic behavior of Problem 21 family", *IEEE Trans. on Magn.*, vol.42, no.4, pp.1467-1470, 2006.
- [8] Z.Cheng, N. Takahashi, S. Yang, C. Fan, M. Guo, L. Liu, J. Zhang, and S. Gao, "Eddy current and loss analysis of multi-steel configuration and validation," *IEEE Trans. on Magn.*, vol.43, no.4, pp.1737-1740, 2007.
- [9] Z.Cheng, N. Takahashi, B. Forghani, G. Gilbert, J. Zhang, L. Liu, Y. Fan, X. Zhang, Y. Du, J. Wang, and C. Jiao, "Analysis and measurements of iron loss and flux inside silicon steel laminations," *IEEE Trans. on Magn.*,vol.45, no.3, pp.1222-1225, 2009.
- [10] Z.Cheng, N.Takahashi, B.Forghani, et al, "Effect of excitation patterns on both iron loss and flux in solid and laminated steel configurations,"*IEEE Trans. on Magn.*, vol.46, no.8, pp.3185-3188, 2010
- [11] Z.Cheng, N.Takahashi, B.Forghani, et al, "Effect of variation of B-H properties on loss and flux inside silicon steel lamination,"*IEEE Trans. on Magn.*, vol.47, no.5, pp.1346-1349, 2011.
- [12] Z.Cheng, N.Takahashi, B.Forghani, L.Liu, Y.Fan, T.Liu, J.Zhang, and X.Wang, "3-D finite element modeling and validation of power frequency multi-shielding effect,"*IEEE Trans. on Magn.*, vol.48, no.2, pp.243-246, 2012.
- [13] Z.Cheng, N.Takahashi, B.Forghani, et al, "*Electromagnetic and Thermal Field Modeling and Application in Electrical Engineering*," Science Press (in Chinese), Beijing, 2009.

- [14] A.J.Moses, "Characterisation and performance of electrical steels for power transformers operating under extremes of magnetisation conditions," *International Colloquium Transformer Research and Asset Management*, Cavtat, Croatia, Nov.12-14, 2009.
- [15] M.Enokizono, H.Shimoji, A.Ikariga, et al, "Vector magnetic characteristic analysis of electrical machines," *IEEE Trans. on Magn.*, vol.41, no.5, pp.2032-2035, 2005.
- [16] K.Fujiwara, T.Adachi, and N.Takahashi, "A proposal of finite-element analysis considering two-dimensional magnetic properties," *IEEE Trans. on Magn.*, vol.38, no.2, pp.889-892, 2002.
- [17] H. Nishimoto, M.Nakano. K.Fujiwara, and N.Takahashi, "Effect of frequency on magnetic properties," *Papers of Technical Meeting on Magnetism, IEE Japan*, MAG-98-56, 1998 (in Japanese).
- [18] J.Zhu, J.J.Zhong, Z.W.lin, et al, "Measurement of magnetic properties under 3-D magnetic excitations," *IEEE Trans. on Magn.*, vol.39, no.5, pp. 3429-3431, 2003.
- [19] J.Turowski, M.Turowski, and M.Kopec, "Method of three-dimensional network solution of leakage field of three-phase transformers," *IEEE Trans. On Magn.*, vol. 26, no. 5, pp. 2911-2919, 1990.
- [20] N.Takahashi, S.Nakazaki, and D.Miyagi, "Optimization of electromagnetic and magnetic shielding using ON/OFF method," *IEEE Trans. on Magn.*, vol.46, no.8, pp.3153-3156, 2010.
- [21] M.Horii, N.Takahashi, and J.Takehara, "3-D optimization of design variables in x-, y-, and z-directions of transformer tank shield model," *IEEE Trans. on Magn.*, vol.37, no.5, pp.3631-3634, 2001
- [22] J. Turowski, X.M. Lopez-Fernandez, A. Soto, and D. Souto, "Stray losses control in core- and shell-type transformers," *Advanced Research Workshop on Transformers*, Baiona, Spain, 29-31 Oct., 2007.
- [23] K.V.Namjosji and P.P.Biringer, "Efficiency of eddy current shielding of structural steel surrounding large currents: a circuit approach," *IEEE Trans. on Magn.*, vol.27, no.6, pp.5417-5419, 1991.
- [24] R.Tang, Y.Li, F.Lin, and L.Tian, "Resultant magnetic fields due to both windings and heavy current leads in large power transformers," *IEEE Trans. on Magn.*, vol.32, no.3, pp.1641-1644, 1996.
- [25] R.M.D.Vecchio, "Eddy current losses in a conducting plate due to a collection of bus bars carrying currents of different magnitudes and phases," *IEEE Trans. on Magn.*, vol.39, no.1, pp.549-552, 2003.
- [26] P.Marketos, S.Zurek, and A.Moses, "A method for defining the mean path length of Epstein," *IEEE Trans. on Magn.*, vol.43, no.6, pp.2755-2757, 2007.
- [27] A.De Rochebrune, J.M.Dedulle, and J.C.Sabonnadiere, "A technique of homogenization applied to the modeling of transformers," *IEEE Trans. on Magn.*, vol. 26, no.2, pp.520-523, 1990.
- [28] H.Kaimori, A.Kameari, and K.Fujiwara, "FEM computation of magnetic field and iron loss using homogenization method," *IEEE Trans.on Magn.*, vol.43, no.2, pp.1405-1408, 2007.
- [29] H.Kaimori, A.Kameari, and K.Fujiwara, "FEM computation of magnetic field and iron loss in laminated iron core using homogenization method," *IEEE Trans. on Magn.*, vol.43, no.4, pp.1405-1408, 2007.
- [30] K.Preis, O.Biro, and I.Ticar, "FEM analysis of eddy current losses in nonlinear laminated iron cores," *IEEE Trans. on Magn.*, vol.41, no.5, pp.1412-1415, 2005.
- [31] T.Kohsaka, N.Takahashi, S.Nogawa, and M.Kuwata, "Analysis of Magnetic characteristics of three-phase reactor model of grain-oriented silicon steel," *IEEE Trans. on Magn.*, vol.36, no.4, pp.1894-1897, 2000.
- [32] H.Igarashi, K.Watanabe, and A.Kost, "A reduced model for finite element analysis of steel laminations," *IEEE Trans. on Magn.*, vol.42, no.4, pp.739-742, 2006.
- [33] O.Biro and K.Preis, "Finite element analysis of 3-D eddy currents," *IEEE Trans. on Magn.*, vol.26, no.2, pp.418-423, 1990.
- [34] O.Biro, K.Preis, and K.R.Richter, "Various FEM formulation for the calculation of transient 3D eddy currents in nonlinear media," *IEEE Trans. on Magn.*, vol.31, no.3, pp.1307-1312, 1995.
- [35] O.Biro, K.Preis, U.Baumgartner, and G.Leber, "Numerical modeling of transformer losses," presented at *International Colloquium Transformer Research and Asset Management*, Cavtat, Croatia, Nov.12-14, 2009.
- [36] J.P.Webb and B.Forghani, "T-Omega method using hierarchical edge elements," *IEE Proc.-Sci.Meas. Technol.*, vol.142, no.2, 1995, pp.133-141.
- [37] Z.Cheng, S.Gao, and L.Li, "Eddy Current Analysis and Validation in Electrical Engineering," Higher Education Press (in Chinese), Beijing, 2001.